

# Synthesis, structure and magnetic properties of $[\text{Fe}^{\text{III}}_4\text{Ln}^{\text{III}}_2]$ (Ln = Gd, Tb, Dy, Ho) and $[\text{Fe}^{\text{III}}_4\text{Y}^{\text{III}}_2]$ clusters

Linh Pham<sup>a</sup>, Khalil A. Abboud<sup>a</sup>, Wolfgang Wernsdorfer<sup>b</sup>, George Christou<sup>a,\*</sup>

<sup>a</sup> Department of Chemistry, University of Florida, Gainesville, FL 32611-7200, United States

<sup>b</sup> Institut Néel, CNRS and Université J. Fourier, BP 166, 38042 Grenoble Cedex 9, France

## ARTICLE INFO

### Article history:

Received 15 February 2013

Accepted 8 April 2013

Available online 18 April 2013

### Keywords:

Iron clusters

Crystal structures

Heterometallic clusters

Magnetic properties

## ABSTRACT

The employment of alcohol-containing chelates and carboxylates in mixed Fe/Ln (Ln = lanthanide) and Fe/Y reactions has afforded a new family of  $[\text{Fe}^{\text{III}}_4\text{Ln}^{\text{III}}_2]$  (Ln = Gd, Tb, Dy, Ho) and  $[\text{Fe}^{\text{III}}_4\text{Y}^{\text{III}}_2]$  clusters. The reaction of  $[\text{Fe}_3\text{O}(\text{O}_2\text{CPh})_6(\text{H}_2\text{O})_3](\text{NO}_3)$ ,  $\text{Ln}(\text{NO}_3)_3$  (Ln = Gd, Tb, Dy, Ho), 2-(hydroxymethyl)pyridine (hmpH) and  $\text{NEt}_3$  in a 1:1:4:4 molar ratio in MeCN/MeOH gave  $[\text{Fe}_4\text{Ln}_2\text{O}_2(\text{hmp})_8(\text{O}_2\text{CPh})_6]$  (Ln = Gd (**1**), Tb (**2**), Dy (**3**), Ho (**4**)). The same reaction with  $\text{Y}(\text{NO}_3)_3$  gave  $[\text{Fe}_4\text{Y}_2\text{O}_2(\text{hmp})_8(\text{O}_2\text{CPh})_6]$  (**5**). The crystal structure of representative complex **1** was solved and reveals a centrosymmetric structure with an  $\text{Fe}_4\text{-Gd}_2$  unit in a chair conformation with the two Gd atoms at opposite ends, above and below an  $\text{Fe}_4$  rectangular plane. Each  $\text{Fe}_2\text{Gd}$  triangle is bridged by a  $\mu_3\text{-O}^{2-}$  ion, and eight hmp<sup>−</sup> groups bind in an  $\eta^1:\eta^2:\mu$  fashion. Ligation is completed by two  $\text{PhCO}_2^-$  group at each Gd, one bound  $\eta^1$  and the other  $\eta^2$ . Analysis of the variable-temperature dc and ac magnetic susceptibility data revealed that the central  $\text{Fe}_4$  rectangular sub-unit has an  $S = 0$  ground state due to strong  $\text{Fe}\cdots\text{Fe}$  exchange interactions, so that at low temperatures the two well separated  $\text{Ln}^{\text{III}}$  behave as magnetically isolated ions. The  $\text{Fe}\cdots\text{Fe}$  interactions were estimated using the magnetostructural correlation reported by Weihe and Güdel, and then determined more accurately from the experimental data for **5**·2H<sub>2</sub>O using the program MAGPACK. The obtained parameters were  $J_1 = -20.5 \text{ cm}^{-1}$  and  $J_2 = -41.3 \text{ cm}^{-1}$ , with  $g$  held constant at 2.0, where  $J_1$  and  $J_2$  are for the  $\text{Fe}\cdots\text{Fe}$  interactions between and within the two  $\text{Fe}_2\text{Y}$  triangles, respectively. The  $\text{Fe}_4\text{Dy}_2$  complex (**3**) exhibits weak out-of-phase signals and very small hysteresis in magnetization versus field scans at low temperature.

© 2013 Elsevier Ltd. All rights reserved.

## 1. Introduction

Research on mixed-metal molecular compounds continues to be stimulated by their relevance to several areas including bioinorganic chemistry, such as the oxygen-evolving center of photosynthesis [1–3], and the nanomagnetism field of single-molecule magnetism and its potential impacts on various established and new technologies [4–6]. In the latter case, heterometallic transition metal/lanthanide (Ln) species have proven to be one of the fastest growing areas for new single-molecule magnets (SMMs) and single-chain magnets (SCMs) [7–16]. SMMs are molecular superparamagnets in which the combination of a large ground state spin ( $S$ ) and a negative zero-field splitting parameter ( $D$ ) results in a significant magnetization relaxation barrier (versus  $kT$ ) at low temperatures. A number of studies have therefore focused on Mn–Ln complexes due to the often ferromagnetic coupling between Mn and Ln atoms [10,13,17,18], the interesting magnetic properties such as spin frustration that they often exhibit [10,18], and not least the intrinsic architectural beauty exhibited by many of these

clusters. Iron–lanthanide (Fe–Ln) chemistry is less well developed, but there is a growing number of studies on the synthesis and characterization of such compounds [19–23]. Unlike high spin  $\text{Mn}^{\text{III}}$ , high-spin  $\text{Fe}^{\text{III}}$  is isotropic and gives strong antiferromagnetic exchange interactions with other  $\text{Fe}^{\text{III}}$ , often leading to small or zero ground state spins. Nevertheless, owing to spin frustration (competing exchange interactions of comparable magnitude), some  $\text{Fe}_x$  topologies can exhibit significant ground state spins, and sometimes even show SMM behavior [21,24–30,31,32].

We have therefore continued our efforts in Fe–Ln cluster chemistry, seeking to develop routes to new examples of such species with perhaps interesting magnetic properties. A general approach that has been successfully employed to make various homo- or heterometallic clusters is the use of alcohol-containing, potentially chelating groups that on deprotonation foster formation of clusters through their alkoxide arms adopting bridging modes and thus promoting a build-up of the product nuclearity [23,28,33,34]. In the present study, 2-(hydroxymethyl)pyridine (hmpH) was chosen because of its well-known ability to yield a variety of transition metal clusters, often with large ground state spin values due to ferromagnetic couplings between metal centers [35,36] and in many cases these are SMMs [37–39]. This ligand has been only

\* Corresponding author. Tel.: +1 352 392 8314; fax: +1 352 392 8757.

E-mail address: [christou@chem.ufl.edu](mailto:christou@chem.ufl.edu) (G. Christou).

modestly employed in iron chemistry [40,41] and surprisingly, there are no examples in Fe–Ln chemistry. We herein report the syntheses, structures and magnetochemical properties of new Fe<sub>4</sub>–Ln<sub>2</sub> clusters (Ln = Gd, Tb, Dy, Ho), and the Fe<sub>4</sub>Y<sub>2</sub> analogue, in which the multiple hmp<sup>−</sup> groups provide the main ligation.

## 2. Experimental

### 2.1. Syntheses

All preparations were performed under aerobic conditions using reagents and solvents as received. [Fe<sub>3</sub>O(O<sub>2</sub>CPh)<sub>6</sub>(H<sub>2</sub>O)<sub>3</sub>](NO<sub>3</sub>) was prepared as described elsewhere [42].

#### 2.1.1. [Fe<sub>4</sub>Gd<sub>2</sub>O<sub>2</sub>(hmp)<sub>8</sub>(O<sub>2</sub>CPh)<sub>6</sub>] (1)

To a stirred solution of hmpH (0.38 ml, 4.0 mmol) in MeCN/MeOH (40/4 ml, v/v) was added Gd(NO<sub>3</sub>)<sub>3</sub> (0.45 g, 1.0 mmol) followed by NEt<sub>3</sub> (0.56 ml, 4.1 mmol). After stirring for 10 min, solid [Fe<sub>3</sub>O(O<sub>2</sub>CPh)<sub>6</sub>(H<sub>2</sub>O)<sub>3</sub>](NO<sub>3</sub>) (0.33 g, 1.0 mmol) was added and the resulting dark orange solution was stirred for 2 h at 70 °C. It was then filtered, and the filtrate was kept undisturbed at room temperature for 3 days. The resulting orange crystals of 1·2H<sub>2</sub>O·0.8MeOH·1.2MeCN were collected by filtration, washed with Et<sub>2</sub>O, and dried in vacuum for three hours; the yield was 60% based on Gd. Dried solid analyzed as 1·2H<sub>2</sub>O. *Anal. Calc.* for C<sub>90</sub>H<sub>82</sub>O<sub>24</sub>N<sub>8</sub>Fe<sub>4</sub>Gd<sub>2</sub>: C, 49.19; H, 3.76; N, 5.09. Found: C, 48.87; H, 3.59; N, 5.05%. Selected IR data (KBr, cm<sup>−1</sup>): 3421(br), 2830(w), 1597(s), 1544(s), 1411(s), 1385(s), 1091(s), 1049(m), 1022(m), 848(m), 759(m), 722(s), 680(m), 643(m), 536(m), 510(m), 458(m) and 421(m).

#### 2.1.2. [Fe<sub>4</sub>Tb<sub>2</sub>O<sub>2</sub>(hmp)<sub>8</sub>(O<sub>2</sub>CPh)<sub>6</sub>] (2)

Complex **2** was prepared similarly to **1** but with Tb(NO<sub>3</sub>)<sub>3</sub> (0.44 g, 1.0 mmol). The yield was ~45%. *Anal. Calc.* for 2·2H<sub>2</sub>O (C<sub>90</sub>H<sub>82</sub>O<sub>24</sub>N<sub>8</sub>Fe<sub>4</sub>Tb<sub>2</sub>): C, 49.12; H, 3.76; N, 5.09. Found: C, 49.32; H, 3.68; N, 4.96%.

#### 2.1.3. [Fe<sub>4</sub>Dy<sub>2</sub>O<sub>2</sub>(hmp)<sub>8</sub>(O<sub>2</sub>CPh)<sub>6</sub>] (3)

Complex **3** was prepared similarly to **1** but with Dy(NO<sub>3</sub>)<sub>3</sub> (0.43 g, 1.0 mmol). The yield was ~45%. *Anal. Calc.* for 3·2H<sub>2</sub>O (C<sub>90</sub>H<sub>82</sub>O<sub>24</sub>N<sub>8</sub>Fe<sub>4</sub>Dy<sub>2</sub>): C, 48.95; H, 3.74; N, 5.07. Found: C, 48.92; H, 3.57; N, 4.96%.

#### 2.1.4. [Fe<sub>4</sub>Ho<sub>2</sub>O<sub>2</sub>(hmp)<sub>8</sub>(O<sub>2</sub>CPh)<sub>6</sub>] (4)

Complex **4** was prepared similarly to **1** but with Ho(NO<sub>3</sub>)<sub>3</sub> (0.44 g, 1.0 mmol). The yield was ~45%. *Anal. Calc.* for 4·2H<sub>2</sub>O (C<sub>90</sub>H<sub>82</sub>O<sub>24</sub>N<sub>8</sub>Fe<sub>4</sub>Ho<sub>2</sub>): C, 48.84; H, 3.73; N, 5.06. Found: C, 48.44; H, 3.61; N, 4.94%.

#### 2.1.5. [Fe<sub>4</sub>Y<sub>2</sub>O<sub>2</sub>(hmp)<sub>8</sub>(O<sub>2</sub>CPh)<sub>6</sub>] (5)

Complex **5** was prepared similarly to **1** but with Y(NO<sub>3</sub>)<sub>3</sub> (0.39 g, 1.0 mmol). The yield was ~45%. *Anal. Calc.* for 5·2H<sub>2</sub>O (C<sub>90</sub>H<sub>82</sub>O<sub>24</sub>N<sub>8</sub>Fe<sub>4</sub>Y<sub>2</sub>): C, 52.45; H, 4.01; N, 5.43. Found: C, 52.29; H, 4.00; N, 5.68%.

### 2.2. General and physical measurements

Elemental analyses (C, H and N) were performed at the in-house facility of the University of Florida Chemistry Department. Infrared spectra in the 400–4000 cm<sup>−1</sup> range were recorded in the solid state (KBr pellets) on a Nicolet Nexus 670 FTIR spectrometer. Variable-temperature DC magnetic susceptibility data down to 5.0 K were collected using a Quantum Design MPMS-XL SQUID susceptometer equipped with a 7 T DC magnet. Pascal's constants were used to estimate the diamagnetic corrections, which were subtracted from the experimental susceptibilities to give the molar

magnetic susceptibilities ( $\chi_M$ ). Microcrystalline samples were re-strained in eicosane to avoid torquing. Ultra-low-temperature (<1.8 K) magnetization hysteresis studies were performed at Grenoble using an array of micro-SQUIDs [43].

### 2.3. X-ray crystallography

X-ray intensity data were collected at 100 K on a Bruker SMART diffractometer using Mo K $\alpha$  radiation ( $\lambda = 0.71073$  Å) and an APEX-II CCD area detector. Raw data frames were read by program SAINT [44] and integrated using 3D profiling algorithms. The resulting data were reduced to produce *hkl* reflections and their intensities and estimated standard deviations. The data were corrected for Lorentz and polarization effects and numerical absorption corrections were applied based on indexed and measured faces. The structure was solved and refined in SHELXTL6.1 [44], using full-matrix least-squares refinement of the *wR*<sub>2</sub> function on *F*<sup>2</sup>. The non-H atoms were refined with anisotropic thermal parameters, and all H atoms were calculated in idealized positions and refined as riding on their parent atoms.

For 1·2H<sub>2</sub>O·0.8MeOH·1.2MeCN, the asymmetric unit consists of a half Fe<sub>4</sub>Gd<sub>2</sub> cluster, an ordered water molecule (O12), and an area of disordered partial MeOH over two positions and a partial MeCN molecule; the MeOH and MeCN total occupancies refined to 0.4 and 0.6, respectively. The H atoms of the water were obtained from a difference Fourier map and refined freely. In the final cycle of refinement, 10069 reflections (of which 8332 are observed with *I* > 2 $\sigma$ (*I*)) were used to refine 604 parameters and the resulting *R*<sub>1</sub>, *wR*<sub>2</sub> and *S* (goodness of fit) were 3.23%, 7.00% and 1.019, respectively. The largest electron density peak is within 0.8 of Gd1 and thus attributed to its anisotropy.

Unit cell data and details of the structure refinement are listed in Table 1.

## 3. Results and discussion

### 3.1. Syntheses

Some of the most common synthetic routes to high-nuclearity Fe<sup>III</sup><sub>*x*</sub> clusters are the reactions of salts containing the oxo-centered triangular cation [Fe<sub>3</sub>O(O<sub>2</sub>CR)<sub>6</sub>(H<sub>2</sub>O)<sub>3</sub>]<sup>+</sup> (R = Me, Et, Ph, etc.) in the presence of potentially chelating groups. The exact identity and

**Table 1**  
Crystallographic data for 1·2H<sub>2</sub>O·0.8MeOH·1.2MeCN.

Parameter	
Formula <sup>a</sup>	C <sub>93.2</sub> H <sub>88.8</sub> Fe <sub>4</sub> Gd <sub>2</sub> N <sub>9.2</sub> O <sub>24.8</sub>
Formula weight (g mol <sup>−1</sup> )	2272.43
Crystal system	monoclinic
Space group	<i>P2</i> <sub>1</sub> / <i>n</i>
<i>a</i> (Å)	12.6107(2)
<i>b</i> (Å)	19.2570(3)
<i>c</i> , Å	18.7576(3)
$\beta$ (°)	90.829(1)
<i>V</i> (Å <sup>3</sup> )	4554.70(12)
<i>Z</i>	2
<i>T</i> (K)	100(2)
Radiation (Å) <sup>b</sup>	0.71073
$\rho_{\text{calc}}$ (g cm <sup>−3</sup> )	1.657
$\mu$ (mm <sup>−1</sup> )	2.137
<i>R</i> <sub>1</sub> <sup>c,d</sup>	0.0441
<i>wR</i> <sub>2</sub> <sup>e</sup>	0.0761

where  $w = 1/[\sigma^2(F_o^2) + (m \cdot p)^2 + n \cdot p]$ ,  $p = [\max(F_o^2, 0) + 2 \cdot F_c^2]/3$ ; *m* and *n* are constants.

<sup>a</sup> Including solvent molecules.

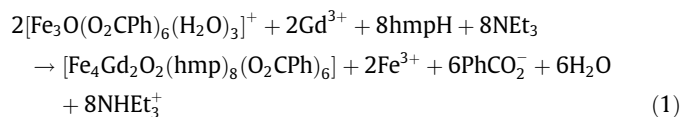
<sup>b</sup> Graphite monochromator.

<sup>c</sup> *I* > 2 $\sigma$ (*I*).

<sup>d</sup>  $R_1 = \Sigma(|F_o| - |F_c|)/\Sigma|F_o|$ .

<sup>e</sup>  $wR_2 = [\Sigma[w(F_o^2 - F_c^2)^2]/\Sigma[w(F_o^2)^2]]^{1/2}$ .

nuclearity of the obtained products can depend on many factors such as the carboxylate, reagent ratios, added base, pH, and the nature and complexity of the chelate, among others. In the present work, we have employed the N,O-chelate hmp<sup>−</sup> and also added a lanthanide salt to the reaction. Various reaction conditions have been investigated by variation of the carboxylate, reagent ratios, and other reaction conditions. In the present work, the reaction of [Fe<sub>3</sub>O(O<sub>2</sub>CPh)<sub>6</sub>(H<sub>2</sub>O)<sub>3</sub>](NO<sub>3</sub>), Ln(NO<sub>3</sub>)<sub>3</sub>, hmpH and NEt<sub>3</sub> in a 1:1:4:4 molar ratio in MeCN/MeOH (10/1 v/v) gave dark orange solutions from which were isolated [Fe<sub>4</sub>Ln<sub>2</sub>O<sub>2</sub>(hmp)<sub>8</sub>(O<sub>2</sub>CPh)<sub>6</sub>] complexes **1–4** in 45–60% yields. The same reaction with Y(NO<sub>3</sub>)<sub>3</sub> gave the corresponding [Fe<sub>4</sub>Y<sub>2</sub>O<sub>2</sub>(hmp)<sub>8</sub>(O<sub>2</sub>CPh)<sub>6</sub>] (**5**) in comparable yield. Complexes **1–5** were concluded to be isostructural on the basis of the elemental analyses and the near superimposable IR spectra. Small changes to the Fe<sub>3</sub>:Ln or MeCN:MeOH ratios for Ln = Gd still gave **1** but led to inferior crystal quality and/or purity. For example, increasing the amount of Fe<sub>3</sub>OBz or MeOH led to **1** precipitating as a microcrystalline powder, and extra Gd(NO<sub>3</sub>)<sub>3</sub> led to contamination of **1** with a white impurity. The NEt<sub>3</sub> is important for the deprotonation of hmpH, but an increase in its amount led to brown oily material we could not characterize. We thus settled for employing the Fe<sub>3</sub>:Ln:hmpH:NEt<sub>3</sub> = 1:1:4:4 stoichiometry to obtain pure, crystalline products even though **1–5** contain a Fe:Ln(Y) = 2:1 ratio. The high reaction temperature was beneficial in overcoming the poor solubility of some of the reactants. The formation of **1** is summarized in Eq. (1).



### 3.2. Description of structures

Since **1–5** were concluded to be isostructural, a full crystal structure determination was carried out only on representative complex **1**·2H<sub>2</sub>O·0.8MeOH·1.2MeCN. The partially labeled structure of **1** is shown in Figs. 1 and 2, and the selected interatomic distances and angles are listed in Table 2. The compound crystallizes in monoclinic space group *P2<sub>1</sub>/n* with the Fe<sub>4</sub>Gd<sub>2</sub> cluster lying on an inversion center. The Fe<sup>III</sup> and Gd<sup>III</sup> atoms are six- and eight-coordinate, respectively, and the molecule can be described as two oxo-centered triangular [Fe<sub>2</sub>Gd(μ<sub>3</sub>-O<sup>2−</sup>)] units with their Fe–Fe edges bridged to each other by four μ<sub>2</sub>-OR<sup>−</sup> alkoxide arms from four η<sup>1</sup>:η<sup>2</sup>:μ-hmp<sup>−</sup> ligands. This gives an Fe<sub>4</sub>Gd<sub>2</sub> chair conformation with the two Gd atoms at two opposite ends and 1.20 Å above and below the Fe<sub>4</sub> plane. The Fe<sub>2</sub>Gd triangles are isosceles, with the Fe–Fe distance (3.552(1) Å) significantly longer than the two Fe–Gd distances (3.442(1) and 3.433 Å). The μ<sub>3</sub>-O<sup>2−</sup> atom O11 has distinctly Y-shaped geometry, with the Fe–O–Fe angle (145.28(11)°) much larger than the Fe–O–Gd angles (106.92(9) and 107.37(9)°). Each Fe–Gd edge is bridged by one of the remaining four hmp<sup>−</sup> groups, which also are η<sup>1</sup>:η<sup>2</sup>:μ with their N atom bound to an Fe atom. Ligation is completed by three benzoate ligands on each Gd atom, two bound in the chelating η<sup>2</sup> and one in the monodentate η<sup>1</sup> fashion. The Fe<sup>III</sup> oxidation states were confirmed by bond valence sum (BVS) calculations (Table 3). The two H<sub>2</sub>O solvent molecules (O12) form two O–H···O hydrogen-bonds with the Fe<sub>4</sub>Gd<sub>2</sub> cluster, to one of the O atoms (O6) of a chelating benzoate (O6···O12 = 2.887(5) Å), and to the unbound O atom (O10) of the monodentate benzoate (O10···O12 = 2.718(5) Å). This strong linkage to the Fe<sub>4</sub>Gd<sub>2</sub> cluster rationalizes why the solvent H<sub>2</sub>O molecules are not lost on vacuum drying, and all five compounds **1–5** analyze as the ·2H<sub>2</sub>O solvates.

The overall structure of **1** is similar to that of [Fe<sub>6</sub>O<sub>2</sub>(hmp)<sub>10</sub>(H<sub>2</sub>O)<sub>2</sub>]<sup>+</sup> reported by Taguchi et al. except that two Fe are replaced by Gd [45]. There are three other [Fe<sub>4</sub>Ln<sub>2</sub>] complexes in the literature [19,20,46], all with distinctly different structures to **1**. The first contains four Fe<sup>III</sup> atoms in a butterfly with each Fe<sub>3</sub> triangle connected to a capping Dy<sup>III</sup> atom; the second contains four Fe<sup>III</sup> and two Dy<sup>III</sup> atoms forming an S-shape topology; and the third has a cyclic structure with two dinuclear Fe<sup>III</sup> units linked by a Ln<sup>III</sup> atom on each side. Thus, the topology of **1** is unprecedented in Fe–Ln chemistry.

### 3.3. Magnetochemistry

#### 3.3.1. Direct current (dc) magnetic susceptibility studies

Solid-state, variable-temperature dc magnetic susceptibility measurements were performed on powdered microcrystalline samples of dried **1**·2H<sub>2</sub>O–**5**·2H<sub>2</sub>O in the 5–300 K range and in a 1 kG (0.1 T) field. The samples were restrained in eicosane to prevent torquing. A summary of the obtained data as χ<sub>M</sub>T versus *T* is presented in Fig. 3 and Table 4.

For **1**·2H<sub>2</sub>O, χ<sub>M</sub>T smoothly decreases from 18.5 cm<sup>3</sup> K mol<sup>−1</sup> at 300 K to 15.2 cm<sup>3</sup> K mol<sup>−1</sup> at 5 K. The value at 300 K is much less than the expected 33.3 cm<sup>3</sup> K mol<sup>−1</sup> for four Fe<sup>III</sup> and two Gd<sup>III</sup> non-interacting atoms. For **2**·2H<sub>2</sub>O–**4**·2H<sub>2</sub>O, χ<sub>M</sub>T decreases from 26.9, 31.6 and 30.4 cm<sup>3</sup> K mol<sup>−1</sup> at 300 K to 17.4, 21.9 and 15.6 cm<sup>3</sup> K mol<sup>−1</sup> at 5 K, respectively. For **5**·2H<sub>2</sub>O containing diamagnetic Y<sup>III</sup> atoms, χ<sub>M</sub>T is only 3.4 cm<sup>3</sup> K mol<sup>−1</sup> at 300 K, indicating strong antiferromagnetic interactions between the Fe<sup>III</sup> atoms, and decreasing to approximately zero (0.06 cm<sup>3</sup> K mol<sup>−1</sup>) at 5 K. In contrast, the Fe–Ln exchange coupling is expected to be very weak, probably less than 1 cm<sup>−1</sup>.

The arrangement of the four Fe atoms in a central rectangular suggests that this fragment of the structure will have an *S* = 0 ground state. A rectangular arrangement of four Fe<sup>III</sup> atoms that are exchange-coupled antiferromagnetically along the edges of the rectangular does not exhibit spin frustration unless there are also significant Fe···Fe interactions along the diagonals of the rectangle or Fe···Ln interactions. The former is not expected in **1–5** since there is no central atom bridging the diagonals, and the Fe···Ln interactions are expected to be too weak to compete with the Fe···Fe interactions. Thus an *S* = 0 ground state is expected for the Fe<sub>4</sub> unit, and the χ<sub>M</sub>T versus *T* data for **5**·2H<sub>2</sub>O in Fig. 3 confirm this. Indeed, even the 300 K χ<sub>M</sub>T is very small at 3.4 cm<sup>3</sup> K mol<sup>−1</sup> (spin-only value for four non-interacting Fe<sup>III</sup> atoms is 17.5 cm<sup>3</sup> K mol<sup>−1</sup>). Extending this analysis to **1–4** therefore suggests that at low temperatures, the two Ln<sup>III</sup> will be non-interacting, since the situation will be akin to two well separated Ln<sup>III</sup> bridged by a long diamagnetic bridging group. Even at 300 K, the observed χ<sub>M</sub>T is expected to be close to that for two Ln<sup>III</sup> free ions plus the small contribution from the Fe<sub>4</sub> unit.

To assess the above analysis, we used the common approach for factoring out the contributions from the heteroatoms in mixed-metal clusters containing Ln<sup>III</sup> atoms, namely subtracting the χ<sub>M</sub>T of the analogue with some diamagnetic metals from the χ<sub>M</sub>T for the paramagnetic analogues. For the present complexes, this difference Δ(χ<sub>M</sub>T) is between **1–4** and **5**, as given in Eq. (2). This approach has been used previously on many occasions in 3d–4f clusters,

$$\Delta(\chi_{\text{M}}T) = \chi_{\text{M}}T(\text{Fe}_4\text{Ln}_2) - \chi_{\text{M}}T(\text{Fe}_4\text{Y}_2) \quad (2)$$

allowing the contributions of the Ln<sup>III</sup> atoms to be factored out [8,47,48]. Similar studies were conducted on Fe<sup>III</sup>–Ln<sup>III</sup> clusters using the isostructural Co<sup>III</sup>–Ln<sup>III</sup> and Fe<sup>III</sup>–La<sup>III</sup> compounds [49], and on Ln<sup>III</sup>–Ln<sup>III</sup> dinuclear systems using Y<sup>III</sup>–Ln<sup>III</sup> and Ln<sup>III</sup>–Y<sup>III</sup> complexes [50,51].

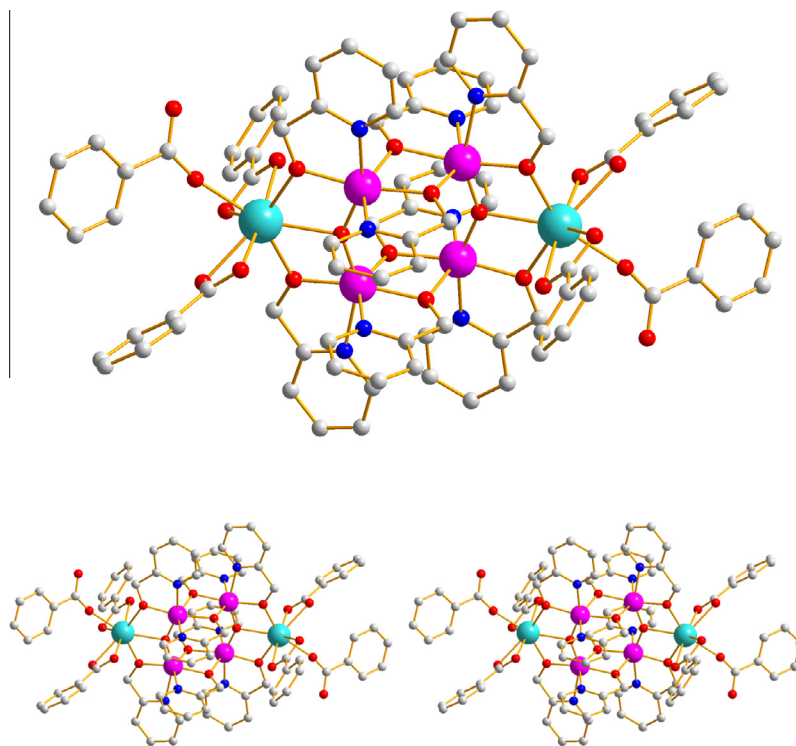


Fig. 1. The structure and stereopair for complex **1**. H atoms have been omitted for clarity. Color code: purple Fe, cyan Gd, O red, N blue, C gray. (Color online.)

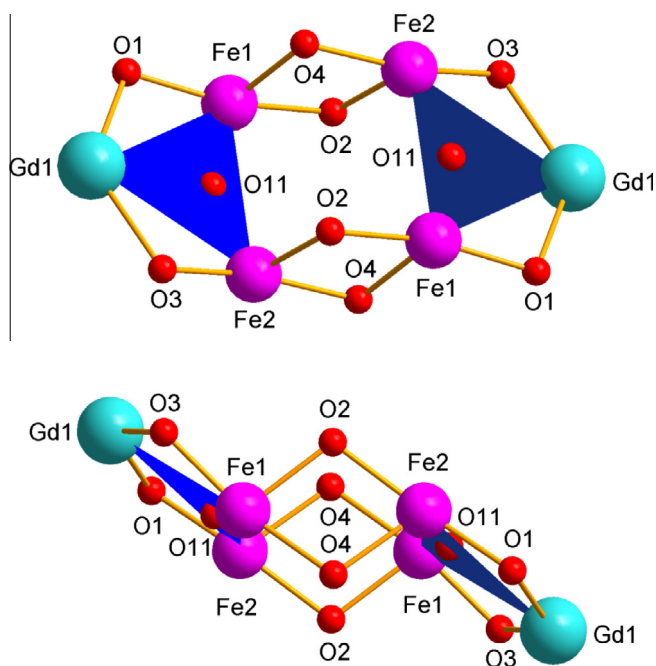


Fig. 2. The labeled core of complex **1** from two essentially perpendicular viewpoints, emphasizing the chair conformation and the oxo-centered triangular units. Color code: purple Fe, cyan Gd, O red. (Color online.)

A plot of  $\Delta(\chi_M T)$  versus  $T$  for **1**·2H<sub>2</sub>O–**4**·2H<sub>2</sub>O is shown in Fig. 4. Of immediate interest is the plot for Fe<sub>4</sub>Gd<sub>2</sub> complex **1**, which is essentially temperature-independent with a  $\Delta(\chi_M T)$  of 15.3 cm<sup>3</sup> K mol<sup>-1</sup>. This is roughly the value expected for two non-interacting isotropic Gd<sup>III</sup> ( $S = 7/2$ ) centers of 15.75 cm<sup>3</sup> K mol<sup>-1</sup> (Table 5), in agreement with the above predictions. For **2–4**, the  $\chi_M T$  (Fig. 3) and  $\Delta(\chi_M T)$  (Fig. 4) plots are temperature-dependent, but the  $\Delta(\chi_M T)$  values at 300 K of 23.4, 28.1 and 27.0 cm<sup>3</sup> K mol<sup>-1</sup>, respectively, are

Table 2  
Selected bond distances (Å) and angles (°) for **1**.

Gd1–O3	2.340(2)	Fe1–O11	1.860(2)
Gd1–O9	2.343(2)	Fe1–O1	1.977(2)
Gd1–O1	2.355(2)	Fe1–O4	2.008(2)
Gd1–O11	2.3933(19)	Fe1–O2	2.027(2)
Gd1–O6	2.422(3)	Fe1–N2	2.158(3)
Gd1–O8	2.446(2)	Fe1–N1	2.221(3)
Gd1–O7	2.464(3)	Fe2–O11	1.861(2)
Gd1–O5	2.547(2)	Fe2–O3	1.970(2)
Fe1–O4–Fe2	106.38(10)	Fe2–O2	2.005(2)
Fe1–O11–Fe2	145.28(11)	Fe2–O4	2.019(2)
Fe1–O11–Gd1	107.37(9)	Fe2–N4	2.174(3)
Fe2–O2–Fe1	106.19(10)	Fe2–N3	2.230(3)
Fe2–O11–Gd1	106.92(9)		

Table 3  
Bond valence sum (BVS)<sup>a</sup> calculations for Fe atoms in **1** and **3**.

Complex	Atom	Fe <sup>II</sup>	Fe <sup>III</sup>
<b>1</b>	Fe1	2.80	<b>3.07</b>
	Fe2	2.77	<b>3.03</b>
<b>3</b>	Fe1	2.84	<b>3.12</b>
	Fe2	2.74	<b>3.12</b>

<sup>a</sup> The bold value is the one closest to the charge for which it was calculated; the oxidation state is the nearest integer to the bold value.

essentially those expected for two isolated Ln<sup>III</sup> free ions. Thus, the decreasing  $\chi_M T$  with temperature for these complexes containing anisotropic Ln<sup>III</sup> centers can be assigned to changing populations of the  $M_J$  states of the  $^{2S+1}\Gamma_J$  ground state.

### 3.3.2. Alternating current (ac) magnetic susceptibility studies

Ac susceptibility data were collected in the 1.8–15 K range using a 3.5 G ac field oscillating at frequencies in the 50–1000 Hz

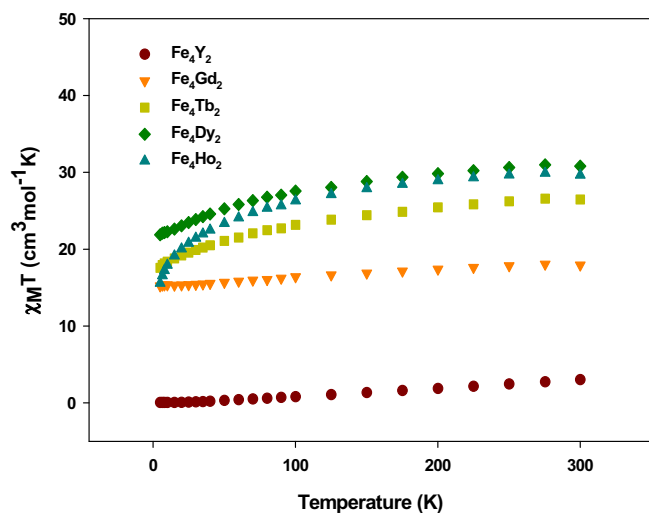


Fig. 3. Plot of  $\chi_{M}T$  vs.  $T$  for 1·2H<sub>2</sub>O–5·2H<sub>2</sub>O.

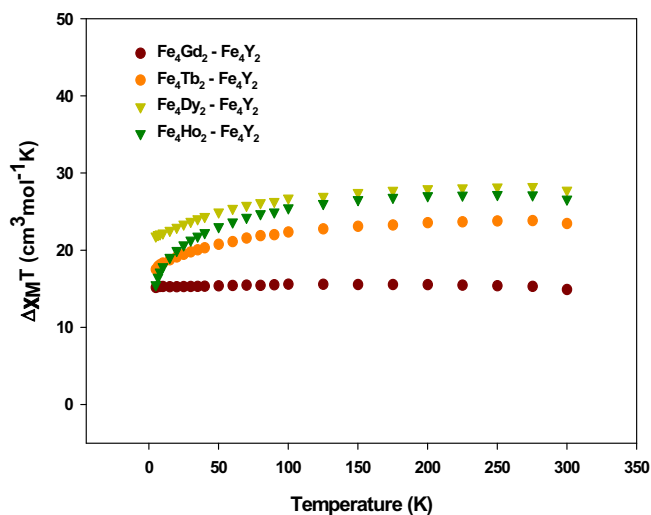


Fig. 4. Plot of  $\Delta(\chi_{M}T)$  vs.  $T$  for 1·2H<sub>2</sub>O–4·2H<sub>2</sub>O.  $\Delta(\chi_{M}T)$  is defined in Eq. (2).

range to probe for possible slow relaxation of the magnetization of 2–4 containing anisotropic Ln<sup>III</sup> ions.

None of the complexes show any frequency-dependent out-of-phase  $\chi''_{M}$  signals down to 1.8 K except the Dy complex 3, which exhibited the tails of peaks lying below 1.8 K (Fig. 5). To probe this further, a single crystal of 3·2H<sub>2</sub>O·0.8MeOH·1.2MeCN (assuming the same solvent content as 1·2H<sub>2</sub>O·0.8MeOH·1.2MeCN) was examined at lower temperatures using a micro-SQUID, but only very small hysteresis loops were detected at 0.04 K (Fig. 6, top), and these showed a scan-rate dependence (Fig. 6, bottom). We conclude that complex 3 is at best only a poor single-molecule magnet with a very small barrier to magnetization relaxation.

### 3.3.3. Determination of the Fe··Fe exchange interactions

The analysis of the dc data above indicated the Fe··Fe interactions were relatively strong and antiferromagnetic, and we sought to determine their magnitude. A rectangular topology is not amenable to the Kambe vector coupling method [52], and we therefore employed two different approaches to obtaining the constituent exchange parameters ( $J$ ) between Fe<sub>2</sub> pairs. We first used the published magnetostructural correlation introduced by Weihe and Güdel in 1997 to determine the  $J$  values of oxo-bridged Fe<sub>2</sub> dinuclear complexes from the metric parameters involving the bridging ligands [53]. The equation developed is given in Eq. (3), where  $J$  is the Fe<sub>2</sub> exchange parameter,  $A = 1.337 \times 10^8$ ,  $B = 3.536$ ,  $C = 2.488$ , and  $D = 7.909$ ,  $\varphi$  is the Fe–O–Fe angle, and  $r$  is the mean Fe–O distance.

$$J = A(B + C \cos \varphi + \cos^2 \varphi) \exp(-Dr) \quad (3)$$

Owing to the centrosymmetric symmetry of 1, this is an exact 2- $J$  system, assuming the diagonal interactions are zero, with the two exchange parameters  $J_1$  and  $J_2$  defined as in Fig. 7. Using the

Table 5

$\chi_{M}T$  for two Ln<sup>III</sup> ions and  $\Delta(\chi_{M}T)$  for the corresponding [Fe<sub>4</sub>Ln<sub>2</sub>].

Ln <sup>III</sup>	Gd <sup>III</sup>	Tb <sup>III</sup>	Dy <sup>III</sup>	Ho <sup>III</sup>
$\chi_{M}T$ for two Ln <sup>IIIa</sup>	15.8	23.6	28.4	28.2
$\Delta(\chi_{M}T)$ at 300 K	15.3	23.4	28.1	27.2
$\Delta(\chi_{M}T)$ at 5 K	15.1	17.3	22.1	15.6

<sup>a</sup> cm<sup>3</sup> K mol<sup>-1</sup>.

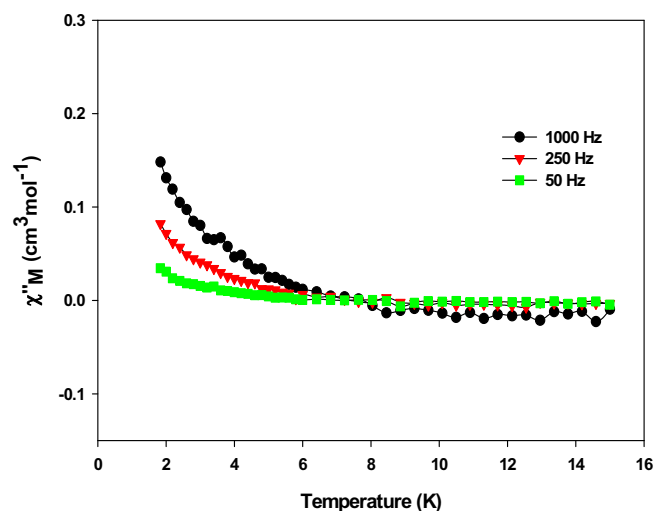


Fig. 5. Plot of the out-of-phase ac susceptibility ( $\chi''_{M}$ ) vs.  $T$  for 3·2H<sub>2</sub>O at the indicated frequencies.

Table 4

Summary of dc magnetic data for complexes 1–5.

Complex	Ln <sup>III</sup> /Y <sup>III</sup> free ion g.s.	$\chi_{M}T$ of Ln <sup>III</sup> free-ion <sup>a</sup>	$\chi_{M}T$ <sup>a</sup> at 5 K	$\chi_{M}T$ <sup>a</sup> at 300 K	$\chi_{M}T$ <sup>a,b</sup> ( $g = 2$ )
[Fe <sub>4</sub> Gd <sub>2</sub> ] (1)	<sup>8</sup> S <sub>7/2</sub>	7.9	15.2	18.5	33.3
[Fe <sub>4</sub> Tb <sub>2</sub> ] (2)	<sup>7</sup> F <sub>6</sub>	11.8	17.4	26.9	41.1
[Fe <sub>4</sub> Dy <sub>2</sub> ] (3)	<sup>6</sup> H <sub>15/2</sub>	14.2	21.9	31.6	45.9
[Fe <sub>4</sub> Ho <sub>2</sub> ] (4)	<sup>5</sup> I <sub>8</sub>	14.1	15.6	30.4	45.7
[Fe <sub>4</sub> Y <sub>2</sub> ] (5)	<sup>1</sup> S <sub>0</sub>	0	0.06	3.4	17.5

<sup>a</sup> cm<sup>3</sup> K mol<sup>-1</sup>.

<sup>b</sup> For non-interacting free ions.

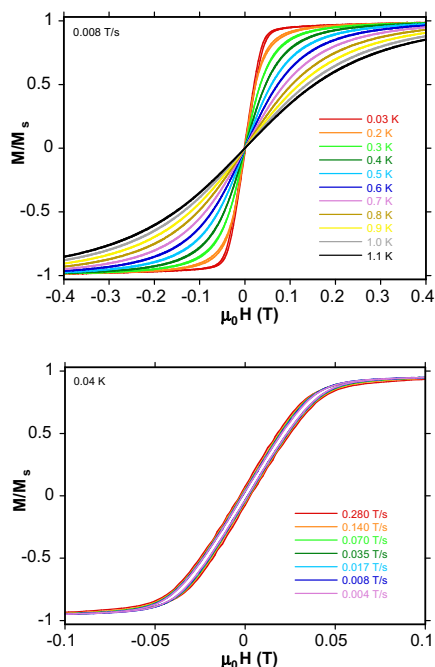


**Fig. 6.** Magnetization ( $M$ ) vs. dc field scans for a single crystal of  $3\cdot 2\text{H}_2\text{O}\cdot 0.8\text{MeOH}\cdot 1.2\text{MeCN}$  at (top) the indicated temperatures with a  $0.008\text{ T/s}$  scan rate, and (bottom) the indicated scan rates at  $0.04\text{ K}$ . The magnetization is normalized to its saturation value,  $M_s$ .

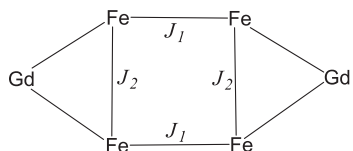


**Fig. 7.** The exchange coupling  $2\text{-}J$  model used to analyze the  $\text{Fe}\cdots\text{Fe}$  interactions in  $1\cdot 2\text{H}_2\text{O}\text{-}5\cdot 2\text{H}_2\text{O}$ .

bond distances and angles in Table 2, we calculated the exchange parameters using Eq. (3) and obtained  $J_1 = -25.3\text{ cm}^{-1}$  and  $J_2 = -59.2\text{ cm}^{-1}$ . The use of a magnetostructural correlation to estimate the  $J$  values thus supports the earlier conclusion that the couplings between the Fe atoms were strongly antiferromagnetic. The factor of two greater magnitude of  $J_2$  versus  $J_1$  is consistent with the larger Fe–O–Fe angle and is as seen previously in e.g., an  $\text{Fe}_6$  cluster [45].

Since the magnetostructural correlation was developed for oxo-bridged  $\text{Fe}_2$  dinuclear complexes, its use on higher nuclearity clusters will likely be less reliable. We tested this by generating the theoretical  $\chi_M T$  versus  $T$  plot for a  $\text{Fe}_4\text{Y}_2$  complex with  $J_1 = -25.3\text{ cm}^{-1}$  and  $J_2 = -59.2\text{ cm}^{-1}$  (Fig. 8, simulation 2) using the program MagPack [54] and comparing it to the experimental dc  $\chi_M T$  versus  $T$  data for  $5\cdot 2\text{H}_2\text{O}$  (Fig. 8, data points). The agreement is clearly very poor; in particular, the simulated line is below the experimental data, indicating the true  $J_1$  and  $J_2$  values for  $5\cdot 2\text{H}_2\text{O}$  to be less negative than given by the magnetostructural correlation. We thus adjusted the  $J_1$  and  $J_2$  values to get a better agreement between the simulation and the experimental data, and excellent agreement was obtained with  $J_1 = -20.5\text{ cm}^{-1}$  and  $J_2 = -41.3\text{ cm}^{-1}$ , with  $g$  held constant at 2.0 (Fig. 8, simulation 1). Although the magnitudes of  $J_1$  and  $J_2$  are  $\sim 20\%$  weaker than those from the magnetostructural correlation, there is still a difference of approximately a factor of two between them.

#### 4. Summary and conclusions

A new family of  $3\text{d-}4\text{f}[\text{Fe}_4\text{Ln}_2]$  ( $\text{Ln} = \text{Gd}, \text{Tb}, \text{Dy}, \text{Ho}$ ) and  $[\text{Fe}_4\text{Y}_2]$  clusters containing the  $\text{hmp}^-$  ligand has been prepared and characterized. The crystal structure of the  $[\text{Fe}_4\text{Gd}_2]$  member shows that the Fe atoms form a central  $\text{Fe}_4$  rectangle with the heterometal atoms attached at either end to give a chair conformation. Magnetically, this is unfortunate because it allows the Fe spins to all couple strongly antiferromagnetically to each other to give a central  $S = 0$  subunit at low temperatures. This leads to the  $\text{Ln}^{\text{III}}$  atoms being magnetically isolated, or in the case of the Y analogue **5**, to an  $S = 0$  molecular spin. The present work emphasizes again the usefulness of the  $\text{hmp}^-$  group as a chelating and bridging ligand, and suggests that further work in this area of mixed-metal cluster chemistry is worth exploring. This is in progress.

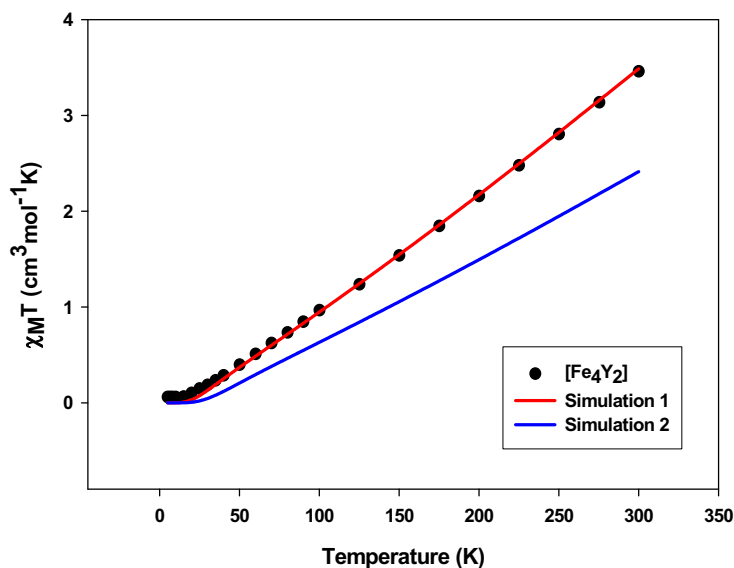


**Fig. 8.** Experimental dc  $\chi_M T$  vs.  $T$  plot for  $5\cdot 2\text{H}_2\text{O}$  (●), and the simulations with  $J_1 = -20.5\text{ cm}^{-1}$  and  $J_2 = -41.3\text{ cm}^{-1}$  (simulation 1), and  $J_1 = -25.3\text{ cm}^{-1}$  and  $J_2 = -59.2\text{ cm}^{-1}$  obtained from the magnetostructural correlation (simulation 2).

## Acknowledgement

This work was supported by the National Science Foundation (DMR-1213030).

## Appendix A. Supplementary data

CCDC 923996 contains the supplementary crystallographic data for **1**·2H<sub>2</sub>O·0.8MeOH·1.2MeCN. These data can be obtained free of charge via <http://www.ccdc.cam.ac.uk/conts/retrieving.html>, or from the Cambridge Crystallographic Data Centre, 12 Union Road, Cambridge CB2 1EZ, UK; fax: (+44) 1223-336-033; or e-mail: [deposit@ccdc.cam.ac.uk](mailto:deposit@ccdc.cam.ac.uk). Supplementary data associated with this article can be found, in the online version, at <http://dx.doi.org/10.1016/j.poly.2013.04.024>.

## References

- [1] K. Wiegardt, U. Bossek, B. Nuber, J. Weiss, J. Bonvoisin, M. Corbella, S.E. Vitols, J.J. Girerd, *J. Am. Chem. Soc.* 110 (1988) 7398.
- [2] J.S. Kanady, E.Y. Tsui, M.W. Day, T. Agapie, *Science* 333 (2011) 733.
- [3] S. Mukherjee, J.A. Stull, J. Yano, T.C. Stamatatos, K. Pringouri, T.A. Stich, K.A. Abboud, R.D. Britt, V.K. Yachandra, G. Christou, *PNAS* 109 (2012) 2257.
- [4] O. Kahn, *Acc. Chem. Res.* 33 (2000) 647.
- [5] R. Bagai, G. Christou, *Chem. Soc. Rev.* 38 (2009) 1011.
- [6] G. Christou, D. Gatteschi, D.N. Hendrickson, R. Sessoli, *MRS Bulletin* 25 (2000) 66.
- [7] S. Osa, T. Kido, N. Matsumoto, N. Re, A. Pochaba, J. Mrozinski, *J. Am. Chem. Soc.* 126 (2003) 420.
- [8] M.L. Kahn, P. Lecante, M. Verelst, C. Mathonière, O. Kahn, *Chem. Mater.* 12 (2000) 3073.
- [9] A. Mishra, W. Wernsdorfer, S. Parsons, G. Christou, E.K. Brechin, *Chem. Commun.* (2005) 2086.
- [10] C. Papatriantafyllopoulou, K.A. Abboud, G. Christou, *Inorg. Chem.* 50 (2011) 8959.
- [11] C.G. Efthymiou, T.C. Stamatatos, C. Papatriantafyllopoulou, A.J. Tasiopoulos, W. Wernsdorfer, S.P. Perlepes, G. Christou, *Inorg. Chem.* 49 (2010) 9737.
- [12] Y.-F. Zeng, G.-C. Xu, X. Hu, Z. Chen, X.-H. Bu, S. Gao, E.C. Sanudo, *Inorg. Chem.* 49 (2010) 9734.
- [13] M. Hołyńska, D. Premužić, I.-R. Jeon, W. Wernsdorfer, R. Clérac, S. Degen, *Chem. Eur. J.* 17 (2011) 9605.
- [14] H.-Z. Kou, S. Gao, X. Jin, *Inorganic Chemistry* 40 (2001) 6295.
- [15] J.-P. Costes, F. Dahan, W. Wernsdorfer, *Inorg. Chem.* 45 (2005) 5.
- [16] M. Estrader, J. Ribas, V. Tangoulis, X. Solans, M. Font-Bardía, M. Maestro, C. Diaz, *Inorg. Chem.* 45 (2006) 8239.
- [17] C. Papatriantafyllopoulou, W. Wernsdorfer, K.A. Abboud, G. Christou, *Inorg. Chem.* 50 (2011) 421.
- [18] A. Saha, M. Thompson, K.A. Abboud, W. Wernsdorfer, G. Christou, *Inorg. Chem.* 50 (2011) 10476.
- [19] S. Nayak, O. Roubeau, S.J. Teat, C.M. Beavers, P. Gamez, J. Reedijk, *Inorg. Chem.* 49 (2009) 216.
- [20] M.N. Akhtar, V. Mereacre, G. Novitchi, J.-P. Tuchagues, C.E. Anson, A.K. Powell, *Chem. Eur. J.* 15 (2009) 7278.
- [21] M. Murugesu, A. Mishra, W. Wernsdorfer, K.A. Abboud, G. Christou, *Polyhedron* 25 (2006) 613.
- [22] M. Ferbinteanu, T. Kajiwara, K.-Y. Choi, H. Nojiri, A. Nakamoto, N. Kojima, F. Cimpoesu, Y. Fujimura, S. Takaishi, M. Yamashita, *J. Am. Chem. Soc.* 128 (2006) 9008.
- [23] A. Baniodeh, I.J. Hewitt, V. Mereacre, Y. Lan, G. Novitchi, C.E. Anson, A.K. Powell, *Dalton Trans.* 40 (2011) 4080.
- [24] T. Taguchi, T.C. Stamatatos, K.A. Abboud, C.M. Jones, K.M. Poole, T.A. O'Brien, G. Christou, *Inorg. Chem.* 47 (2008) 4095.
- [25] R. Bagai, M.R. Daniels, K.A. Abboud, G. Christou, *Inorg. Chem.* 47 (2008) 3318.
- [26] R. Bagai, K.A. Abboud, G. Christou, *Inorg. Chem.* 46 (2007) 5567.
- [27] S. Mukherjee, R. Bagai, K.A. Abboud, G. Christou, *Inorg. Chem.* 50 (2011) 3849.
- [28] R. Bagai, K.A. Abboud, G. Christou, *Chem. Commun.* (2007) 3359.
- [29] K. Weighardt, K. Pohl, I. Jibril, G. Huttner, *Angew. Chem. Int. Ed. Engl.* 23 (1984) 77.
- [30] D. Gatteschi, M. Fittipaldi, C. Sangregorio, L. Sorace, *Angew. Chem. Int. Ed. Engl.* 51 (2012) 4792.
- [31] S. Schmidt, D. Prodius, V. Mereacre, G.E. Kostakis, A.K. Powell, *Chem. Commun.* (2013).
- [32] D. Schray, G. Abbas, Y. Lan, V. Mereacre, A. Sundt, J. Dreiser, O. Waldmann, G.E. Kostakis, C.E. Anson, A.K. Powell, *Angew. Chem. Int. Ed. Engl.* 49 (2010) 5185.
- [33] J.T. Brockman, T.C. Stamatatos, W. Wernsdorfer, K.A. Abboud, G. Christou, *Inorg. Chem.* 46 (2007) 9160.
- [34] T. Taguchi, M.S. Thompson, K.A. Abboud, G. Christou, *Dalton Trans.* 39 (2010) 9131.
- [35] N.C. Harden, M.A. Bolcar, W. Wernsdorfer, K.A. Abboud, W.E. Streib, G. Christou, *Inorg. Chem.* 42 (2003) 7067.
- [36] T.C. Stamatatos, K.A. Abboud, W. Wernsdorfer, G. Christou, *Angew. Chem. Int. Ed. Engl.* 45 (2006) 4134.
- [37] T.C. Stamatatos, K.A. Abboud, W. Wernsdorfer, G. Christou, *Angew. Chem. Int. Ed. Engl.* 46 (2007) 884.
- [38] C. Boskovic, E.K. Brechin, W.E. Streib, K. Folting, J.C. Bollinger, D.N. Hendrickson, G. Christou, *J. Am. Chem. Soc.* 124 (2002) 3725.
- [39] T. Taguchi, W. Wernsdorfer, K.A. Abboud, G. Christou, *Inorg. Chem.* 49 (2010) 10579.
- [40] C.A. Christmas, H.L. Tsai, L. Pardi, J.M. Kesselman, P.K. Gantzel, R.K. Chadha, D. Gatteschi, D.F. Harvey, D.N. Hendrickson, *J. Am. Chem. Soc.* 115 (1993) 12483.
- [41] E.K. Brechin, M.J. Knapp, J.C. Huffman, D.N. Hendrickson, G. Christou, *Inorg. Chim. Acta*, 297 (2000) 389.
- [42] A. Earnshaw, B.N. Figgis, J. Lewis, *J. Chem. Soc. (A)* (1966) 1656.
- [43] W. Wernsdorfer, in: *Adv. Chem. Phys.*, 2001, pp. 99.
- [44] SHELXTL6 (2008). Bruker-AXS, Madison, Wisconsin, USA.
- [45] Taguchi, T. A molecule approach to nanoscale magnetic materials: New iron and manganese clusters from the use of pyridyl alcohol, PhD Dissertation, (2009).
- [46] S. Schmidt, D. Prodius, G. Novitchi, V. Mereacre, G.E. Kostakis, A.K. Powell, *Chem. Commun.* 48 (2012) 9825.
- [47] M.L. Kahn, C. Mathonière, O. Kahn, *Inorg. Chem.* 38 (1999) 3692.
- [48] J.-P. Costes, F. Dahan, A. Dupuis, J.-P. Laurent, *Chem. Eur. J.* 4 (1998) 1616.
- [49] A. Figuerola, C. Diaz, J. Ribas, V. Tangoulis, J. Granell, F. Lloret, J. Mahía, M. Maestro, *Inorg. Chem.* 42 (2002) 641.
- [50] N. Ishikawa, T. Iino, Y. Kaizu, *J. Am. Chem. Soc.*, 124 (2002) 11440.
- [51] J.-P. Costes, F. Dahan, F. Nicodème, *Inorg. Chem.* 40 (2001) 5285.
- [52] K.J. Kambe, *Phys. Soc. Jpn.* 5 (1950) 48.
- [53] H. Weihe, H.U. Güdel, *Am. Chem. Soc.* 119 (1997) 6539.
- [54] MAGPACK - J.J. Borrás-Almenar, J. M. C.-J., E. Coronado, B. Tsukerblat, Departamento de Química, Universidad de Valencia, Valencia, Spain, (2000).